ACS OMEGA

http://pubs.acs.org/journal/acsodf

Article

Enhancing the Catalytic Properties of Mordenites via an Alkali–Acid Treatment and by Loading Nickel–Cerium during *o*-Ethyltoluene Isomerization

Xiaoyan Cao, Ruiyun Wang, Kaijun Wang, Zhenggui Gu,* and Fang Wang*

Cite This: *ACS Omega* 2021, 6, 22688–22699

Read Online

ACCESS | Metrics & More | Article Recommendations

ABSTRACT: The catalytic performance of the selective isomerization of *o*-ethyltoluene (O-ET) is crucial to increasing the *m*-ethyltoluene (M-ET) and *p*-ethyltoluene (P-ET) yields. During the isomerization of O-ET, traditional (commercial) mordenites (HM) are generally limited by a high reaction temperature (235 °C), as well as a low yield of the isomerization product (49.0%). In this study, micro-mesoporous mordenites were obtained by treating commercial mordenites with NaOH, NaOH–HNO_3, and NaOH–mixed acid (HNO_3–oxalic). Thereafter, their structure, porosity, and acidity were investigated via X-ray diffraction, transmission electron microscopy, inductively coupled plasma, N_2 sorption, X-ray photoelectron spectroscopy, Fourier transform infrared spectroscopy of pyridine, temperature-programmed desorption of ammonia, and nuclear magnetic resonance. Among the various treated samples, the accessibility of the acidic sites and the *B*/*L* value of the alkali–mixed HNO_3–oxalic one were enhanced, achieving the highest yield (53.6%) and lowest reaction temperature (165 °C), thus significantly reducing the energy consumption of the reaction process. Furthermore, Ni and Ce were successfully loaded via the incipient wetness impregnation of the micro-mesoporous mordenite to significantly prolong the catalytic life. This study affords a new strategy for obtaining high M-ET and P-ET yields from the isomerization of O-ET in mixed C_9 aromatics on an industrial scale.

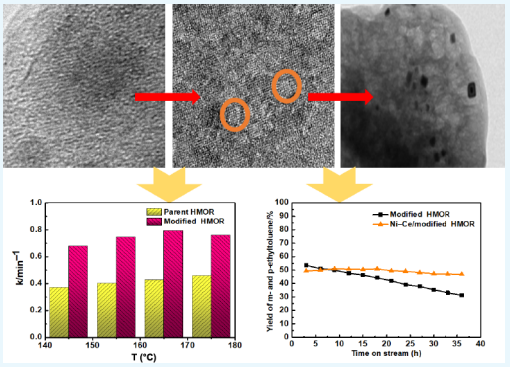

INTRODUCTION

Owing to the scarcity of natural resources, it has become urgent to improve the conversion and utilization rates of chemical products. The bottom oil of the xylene column in a refinery contains many C_9 aromatics, including ethyltoluene, trimethylbenzene (TMB), and tetramethylbenzene.[1,2] Specifically, *o*-ethyltoluene (O-ET) can be isomerized into *m*-ethyltoluene (M-ET) and *p*-ethyltoluene (P-ET), after which poly(methylstyrene), which is an essential raw material for fabricating functional materials, can be obtained through dehydrogenation and polymerization reactions. Additionally, O-ET in C_9 aromatics could inhibit the purification of 1,3,5-TMB, which is an essential resource material for synthesizing fine chemicals.[3,4] Thus, it is necessary to improve the conversion rate of O-ET, which could subsequently increase the yields of M-ET and P-ET and reduce the content of O-ET.

Hydrogen-type mordenite (HMOR) molecular sieves have been recently employed as effective catalysts for the isomerization of O-ET owing to their higher conversion rate and selectivity compared with HZSM-5, H*β*, and ammonium silicotungstate, as well as ammonium phosphotungstate.[5−8] Meier[9] observed the two-dimensional structure of mordenite in 1961 and deduced that the effective diameter of the 12-membered ring channel of HMOR was between 8.2 and 8.6 Å (slightly larger than that of the ethyltoluene isomers, which was determined from the Fisher–Hirschfelder–Taylor molecular models.[10] However, the ethyltoluene molecule could barely pass through the eight-membered ring pore owing to the effective aperture of mordenite (2.6 × 5.7 Å, Figure 1), which only exhibited a one-dimensional pore structure.[10] Therefore, the structure of this commercial mercantile zeolite reveals that the acidic sites in the pores were underutilized, the conversion of O-ET at low temperatures was low, and the macromolecular byproducts could not be readily diffused out of the pores owing to hindrance. These factors could cause the rapid coking and deactivation of the catalyst, thereby limiting its industrial-scale application.[11−14] Hence, it is essential to obtain high-efficiency catalysts by optimizing the porosity and acidity of commercial mordenites (HM).

Generally, meso-microporous mordenites can be mainly prepared by removing the Al and Si frameworks via NaOH

Received: May 29, 2021
Accepted: August 19, 2021
Published: August 25, 2021

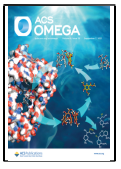

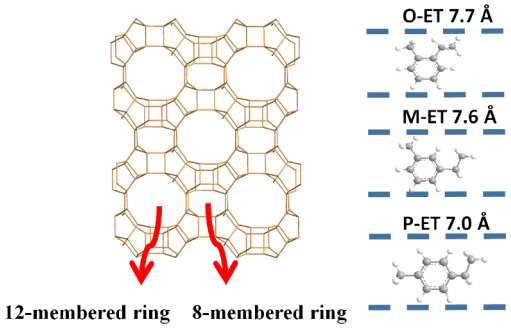

Figure 1. Illustration of the mordenite structure (left) and the kinetic diameter (right) of ethyltoluene, which is determined from the Fisher–Hirschfelder–Taylor molecular models. Adapted with permission from ref 10. Copyright 1970 Elsevier.

desilication, which is the most employed and inexpensive method for transforming micropores into intracrystalline mesopores in zeolites.[15−18] However, many researchers[19−21] have indicated that some nonframeworks of the Al species can be deposited on the outer surface of the zeolite framework during alkali-treatment-based desiliconization and can even block the pores and lower its acidity and catalytic activities. Therefore, pickling treatments employing acids, such as HCl, HNO_3, and oxalic acid, were required to wash off the nonframework Al species. Giudici et al.[22] observed that oxalic acid, a stronger dealumination agent than HNO_3, exerted a greater effect on the framework structure than HNO_3; it mainly removed the nonframework Al and increased the B/L ratio. However, oxalic acid removed the nonframework Al and extracted a part of the Al framework because of its chelation.[23] Evidently, during the pickling process, the different impacts of the acids on the structure, as well as the acidity of zeolites, were demonstrated. Our previous investigations[24] also revealed that a mixture of organic (oxalic acid) and inorganic (HCl) acids could effectively improve the specific surface area (SSA), pore volume, and B/L ratio of the molecular sieve, thus endowing it with good catalytic performance. Nevertheless, there are no reports on the dealumination of HMOR by mixed HNO_3−oxalic acids.

Furthermore, the loading of metals onto zeolites, followed by hydrogenation, could cause the easy cracking of coked aromatic rings to relieve coking and improve the stability of the catalyst.[25] Pt and Pd, which are expensive, are easily poisoned by S, N, and As. Thus, they are being gradually replaced by transition and rare-earth metals, such as Ni, Mo, Cu, W, La, and Ce.[26−29] Wang et al.[30] believed that the catalyst life could be significantly increased by loading Ni−Mo or Ni−La on HMOR. Ning et al.[31] indicated that the introduction of Ce could effectively inhibit the aggregation of Pt during the isomerization of *n*-dodecane. The isomerization of O-ET catalyzed by micro-mesoporous HMOR loading of Ni−Ce has not been reported.

In this study, a secondary mesoporous structure was introduced into commercial mordenites via a post-treatment method while preserving its original microporous structure. Moreover, the effects of alkali and alkali−acid post-treatment on the structure, porosity, and acidity of the micro−mesoporous mordenite were discussed. Furthermore, the stability of the catalyst was investigated by loading Ni and Ce onto the micro−mesoporous mordenite. Finally, the isomerization reaction of O-ET in mixed C_9 aromatics was considered as the research object, and the performances of the catalysts, which were obtained via the various modification processes, were evaluated for the first time. Our research affords a new strategy for increasing the M-ET and P-ET contents in C_9 aromatics, thus reducing the consumption of the production energy and promoting the development of green chemistry.

RESULTS AND DISCUSSION

Catalyst Selection. The isomerization performances[32−34] of O-ET in the C_9 aromatic mixture were tested in the presence of the parent and modified mordenites (Figure 2).

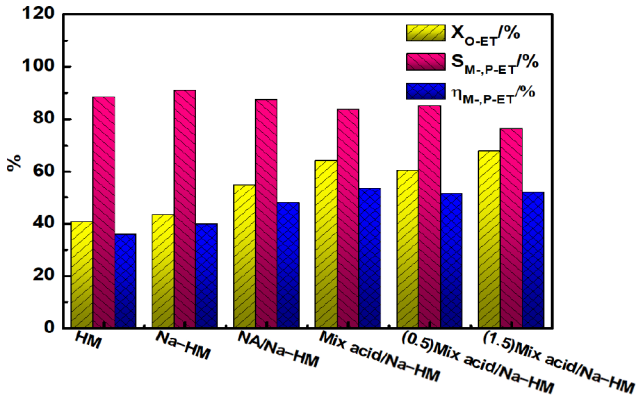

Figure 2. Results of O-ET isomerization employing different catalysts. The data were the averages of three experiments, and the maximum standard deviation of each data was <2.0%.

The catalytic performance of the modified mordenite was evidently better than that of the parent one. In particular, the presence of Mix acid/Na−HM mordenite ensured that M-ET and P-ET were obtained in the highest yield compared with the yield of the other samples. Moreover, a certain synergy might exist between HNO_3 and oxalic acid during the modification; the ratio between them is also crucial. Therefore, the Mix acid/Na−HM was selected as the catalyst for further research.

Physicochemical and Structural Properties. The X-ray diffraction (XRD) patterns of the parent and modified HM zeolite samples are shown in Figure 3. The patterns exhibit the characteristic diffraction peaks of the HM zeolite, and slight differences were observed in the intensities of the peaks at 2θ

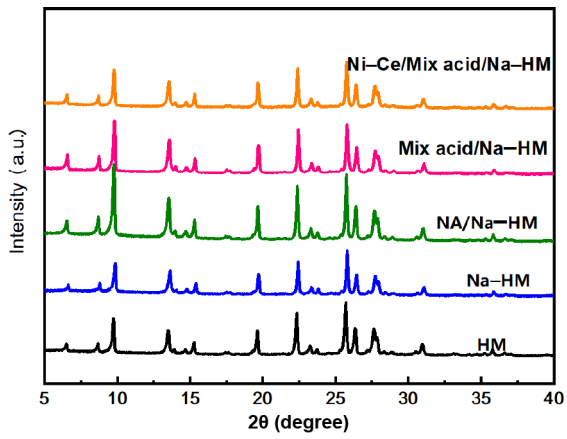

Figure 3. XRD patterns of the parent and modified HM samples.

https://doi.org/10.1021/acsomega.1c02809
ACS Omega 2021, 6, 22688−22699

of 5°−30°, demonstrating that the crystal integrity of the HM zeolite was well-preserved. Assuming that the crystallinity of the parent HM was 100%, the relative crystallinity of the sample was calculated based on the total areas of the characteristic diffraction peaks between 2θ = 5° and 30°.[35] The crystallinity of the Na−HM sample decreased to 85%, indicating the relatively significant effect on the crystallinity of alkali treatment (Table 1). Moreover, the erosion of the HM zeolite from the alkaline solution might cause the extraction of the Si and Al amorphous species from the parent HM framework, resulting in the collapse of a part of the framework, as also observed by Hunag et al.[20] Contrary to the Na−HM sample, the relative crystallinities of the NA/Na−HM and Mix acid/Na−HM samples were better preserved. These results revealed that the alkali treatment process exerted a stronger influence on the long-range ordering of the zeolite compared with the acid treatment one.[20] Additionally, the characteristic peaks of mordenite, as obtained via XRD, appeared clearly in the Ni−Ce catalysts that were supported on micro-mesoporous mordenite, indicating that the structure of mordenite was preserved after loading the metals. Ni−Ce/Mix acid/Na−HM did not exhibit any apparent diffraction peak that was assignable to the Ni and Ce species since their small sizes in the modified HM prevented the diffractometer from detecting their patterns.[36] Thus, the subsequent SEM mapping and X-ray photoelectron spectroscopy (XPS) results would be discussed in further detail.

Figure 4 shows the N_2 sorption isotherms and pore-size distribution (PSD) (inset) of the HM and modified HM samples. Surprisingly, the parent mordenite HM sample exhibits compound characteristics of type I and type IV hysteresis loops in the sorption isotherms, indicating the presence of the mesopores. Generally, the typical sizes of commercial mordenite crystals are between 100 and 200 nm, which readily form larger particle aggregates and promote the formation of intergranular mesopores.[37] Moreover, the rapid adsorption of N_2 at low relative pressures ($P/P_0 < 0.05$) of the modified samples indicates the preservation of the micropores. The stability of the modified mordenite depended on the preservation of the microporous structure of the parent mordenite, and this finding is consistent with the XRD results. The samples display a significant hysteresis loop at a higher relative pressure, thereby confirming the presence of the mesopores. Simultaneously, the PSD diagram (inset) reveals that the average pore diameters of HM, Na−HM, and Mix acid/Na−HM increase sequentially. Notably, Table 1 reveals the following after alkali treatment: the SSA of the sample decreased from 482 to 453 $m^2\ g^{-1}$, the external surface area increased from 25 to 33 $m^2\ g^{-1}$, the micropore volume decreased from 0.180 to 0.161 $m^3\ g^{-1}$, and the mesopore volume increased from 0.047 to 0.066 $m^3\ g^{-1}$. These results indicate that the mesopores were formed by sacrificing the micropores.[38] The micropores were transformed into mesopores during alkali treatment, although the increase in the mesopores was insignificant.[39,40] Since the alkali treatment could cause the collapse of a part of the framework structure, the formed amorphous Si and nonframework Al species might block the pores, as demonstrated by the XRD results. Sazama et al.[39] reported that the extraction of Si from the parent HM framework could cause the collapse of the walls of the micropores, thus causing a significant reduction in the area of the micropores. Compared with NA/Na−HM, the Mix acid/Na−HM with a higher pore volume and SSA demonstrated

Table 1. Structural Properties and Chemical Compositions of the Parent and Modified HM Samples

sample	relative crystallinity (%)	Si/Al[d]	S_{BET} ($m^2\ g^{-1}$)[a]	S_{ext} ($m^2\ g^{-1}$)[b]	S_{micro} ($m^2\ g^{-1}$)[b]	S_{meso} ($m^2\ g^{-1}$)[c]	V_{micro} ($cm^3\ g^{-1}$)[b]	V_{meso} ($cm^3\ g^{-1}$)[c]	pre-exponential factor A	I (%)[e]		
										SiOH	Si (3Si, 1 Al)	Si (4Si)
HM	100	12.8	482	25	457	14	0.180	0.047	1.98	2.6	32.2	65.2
Na−HM	85	9.0	453	33	420	21	0.161	0.066	3.18	2.2	31.9	65.9
NA/Na−HM	115	12.6	516	122	393	54	0.166	0.145	4.46		n.d.[f]	
Mix acid/Na−HM	108	13.1	559	130	429	64	0.172	0.161	7.64	2.3	27.1	70.6
Ni−Ce/Mix acid/Na−HM	n.d.	n.d.	522	115	417	55	0.170	0.148	n.d.	n.d.		

[a]BET method. [b]t-Plot method. [c]Barrett−Joyner−Halenda method (the adsorbtion branch). [d]ICP−OES method. [e]Proportion of different Si types. [f]n.d., not determined.

https://doi.org/10.1021/acsomega.1c02809
ACS Omega 2021, 6, 22688−22699

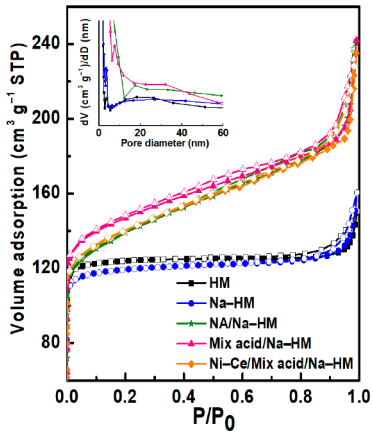

Figure 4. N_2 adsorption−desorption isotherms and PSDs (inset) of the parent and modified HM samples.

that the addition of oxalic acid could significantly promote the change in the structure of the mordenite. These results demonstrate that the mild retreatment employing the mixed acid, following alkali treatment, could significantly enhance the SSA, external surface area, and mesoporous volume, thus improving mass transfer. Additionally, the Brunauer−Emmett−Teller (BET) surface area and mesopore volume of the Mix acid/Na−HM were reduced by 6.6% and 8.07%, respectively, after loading Ni and Ce, indicating that the structural properties of the micro-mesopore mordenite were only slightly affected by the metal loading.

Table 1 presents the molar ratios of the bulk Si/Al of the catalysts, as obtained via inductively coupled plasma (ICP) measurements. The molar ratio of Si/Al of HM was higher and lower than those of Na−HM and Mix acid/Na−HM, respectively, indicating that the alkali accounted for the dissolution of Si in the HM samples, while the mild mixed acid accounted for dealumination. Moreover, a high molar ratio of Si/Al for the Mix acid/Na−HM sample demonstrated that the mixed acid exerted a stronger dealumination effect.

The ^{27}Al and ^{29}Si magic-angle spinning nuclear magnetic resonance (MAS-NMR) spectra were recorded to obtain the coordination states of the Si and Al species in the parent and modified HM samples (Figure 5). Figure 5a shows the strong and weak peaks, which corresponded to the tetrahedrally and octahedrally coordinated Al framework and nonframework, at ∼54 and 0 ppm, respectively, indicating that the framework Al was the main form.[41] The content of the nonframework Al species increased from 16.3% to 23.4% via alkali treatment and then decreased to 9.9% after the alkali−mixed acid treatments (Table 2). The result indicates that the alkali treatment can facilitate the transformation of a part of the framework Al into a nonframework species, which can be readily removed via the mixed-acid treatment. The ^{29}Si MAS-NMR spectrogram reveals that they are chiefly composed of different tetrahedral sites (Figure 5b). The fitting peak of the ^{29}Si spectrum

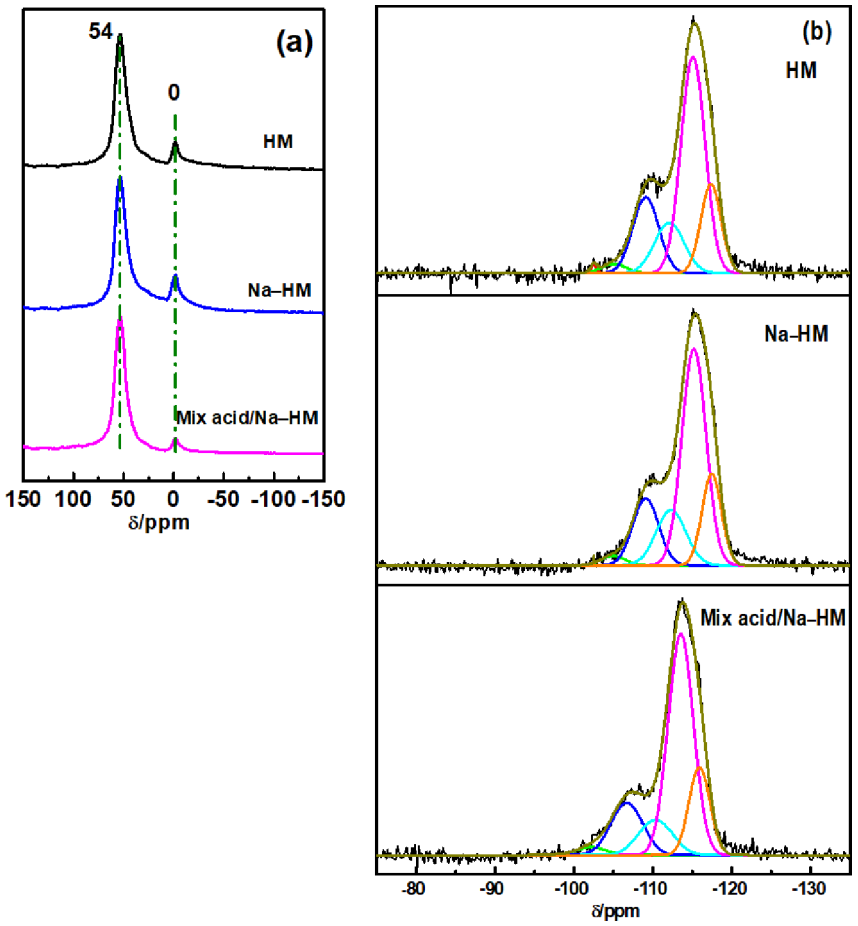

Figure 5. (a) ^{27}Al and (b) ^{29}Si MAS-NMR spectra of the parent and modified HM samples. The peak signals were fit according to ref 41. Adapted with permission from ref 41. Copyright 2013 Elsevier.

https://doi.org/10.1021/acsomega.1c02809
ACS Omega 2021, 6, 22688−22699

Table 2. Acid Contents and Properties of the Parent and Modified HM

sample	peak temperature (°C)[a]		acid contents ($cm^3\ g^{-1}$)[a]			B/L[b]	I (%)[c]	P-ET/M-ET[d]
	T_1	T_2	weak acid	strong acid	total acid			
HM	198	446	14.1	37.0	51.1	4.9	16.3	0.41
Na−HM	203	421	16.8	35.8	52.6	3.0	23.4	0.40
Mix acid/Na−HM	171	461	13.8	48.8	62.5	10.1	9.9	0.38
Ni−Ce/Mix acid/Na−HM	178	450	13.9	48.1	62.0	8.1	n.d.[e]	n.d.

[a]NH_3-TPD method. [b]Py-FTIR method. [c]Relative intensity of the octahedral Al types. [d]Ratio of P-ET to O-ET isomers. [e]n.d., not determined.

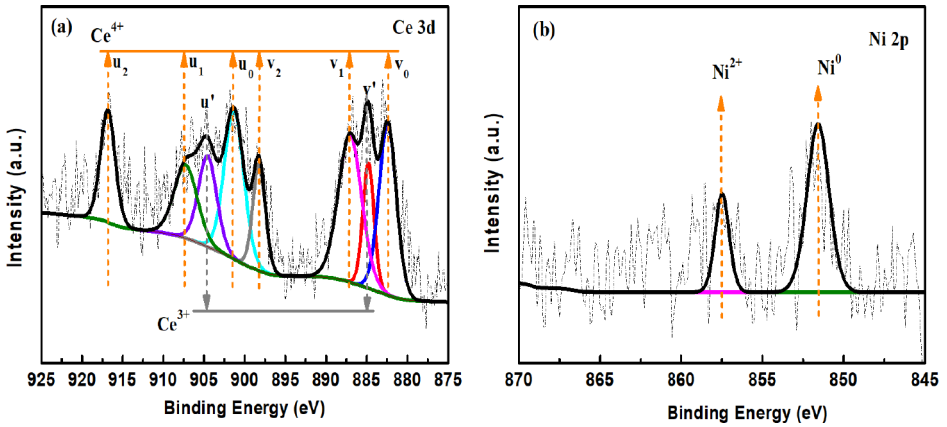

Figure 6. XPS spectra of the Ni−Ce/Mix acid/Na−HM sample: (a) Ce 3d and (b) Ni 2p. The binding energy error is <0.3 eV for two scans.

consisted of six peaks in the ranges of −97.0 to −103.0 ppm (SiOH), −106.0 to −110.5 ppm [Si (3Si, 1Al)], and −112.0 to −116.0 ppm [Si (4Si)].[41] Since the negatively charged AlO^{4-} tetrahedron can prevent the hydrolysis of the Si−O−Al bonds by OH−,[42] the alkali treatment will mainly cause the leaching of the Si (4Si) species, thus probably increasing the proportion of the Si (3Si, 1Al) site in Na−HM. However, the proportion of Si (4Si) to Si (3Si, 1Al) barely changed (Table 1) during the alkali desilication process since they both decreased, and the result conformed to that of ^{27}Al MAS-NMR analyses (Figure 5a). Additionally, the proportion of the Si (3Si, 1Al) sites in the Mix acid/Na−HM was slightly lower than that in the Na−HM sample (Table 1), and this could be attributed to the fact that mild mixed-acid treatment favored the removal of the nonframework aluminum and caused the leaching of some framework Al, further fully reflecting the roles of HNO_3 and oxalic acid, and this finding agrees well with the N_2-sorption result.

The charge states of Ni and Ce species, which were loaded into the micro−mesoporous Mix acid/Na−HM, were analyzed via XPS. Figure 6a shows the Ce 3d energy. By fitting the curve, the Ce 3d spectrum was divided into two sets of spin−orbit multiplets:[43] Ce 3d3/2 and Ce 3d5/2, which were marked as "u" and "v", respectively. u_0, u_1, and u_2 represent Ce^{4+} 3d5/2 and v_0, v_1, and v_2 represent Ce^{4+} 3d3/2, where u_2 and v_2 correspond to the Ce^{4+} $3d^{10}4f^0$ orbital.[44] Additionally, u' and v' represent the Ce^{3+} 3d5/2 and Ce^{3+} 3d3/2 spectra, which correspond to the Ce^{3+} $3d^{10}4f^1$ orbital, respectively. Figure 6b shows the energy spectrum of Ni 2p in which the binding energies, 852.6 and 856 eV, were attributed to Ni^0 and Ni^{2+},[45] respectively, indicating that CeO_2 was partially reduced to Ce^{3+} during the H_2-reduction process, while the partial Ce^{4+} state was preserved. The presence of CeO_2 could prevent the aggregation of NiO in the calcination process and improve the dispersion of NiO.[46] Ni mainly existed as Ni^0, which availed sufficient metal sites for the hydrogenation reaction to alleviate the coking of the catalyst during the reaction.[28] A small amount of Ni^{2+} might exist because the unique electron transfer produced Ni and afforded positively charged electrons to the surface as Ni^{2+}[31,47] when Ni interacted with CeO_2.[31,47]

Characterization of the Acidity. The number of the acid centers in the catalyst, as well as its strength, was measured via temperature-programmed desorption of ammonia (NH_3-TPD). Two major NH_3-desorption peaks were observed in the ranges of 150−250 °C (T_1) and 250−500 °C (T_2) (Figure 7), corresponding to the weak and strong acid sites,

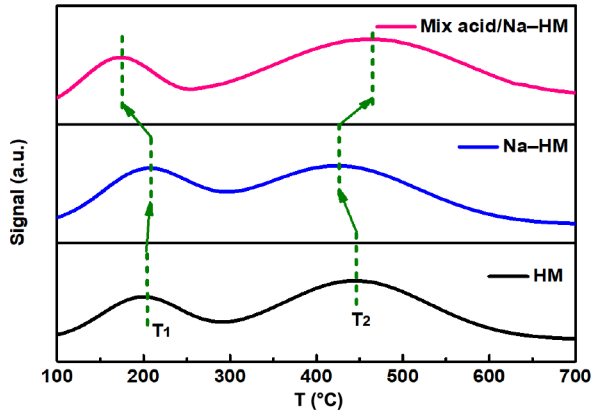

Figure 7. NH_3-TPD profiles of the parent and modified HM samples.

respectively.[48] Based on the peak areas, the amounts of the weak, strong, and total acids were quantitatively obtained (Table 2).[49] It was observed that the position of the desorption peak of the strong acid shifted to the low-temperature region after NaOH desilication; however, it shifted to a high-temperature region after mild treatment, employing the

https://doi.org/10.1021/acsomega.1c02809
ACS Omega 2021, 6, 22688−22699

mixed acid. Combined with the structural characterization results, the tetrahedral-framework Al was inevitably removed during the alkali treatment, thereby weakening the strong-acid site.[50] The acid treatment removed the nonframework Al, and this could strengthen the strong-acid sites.[51] The total acid of Na−HM did not increase significantly, although it exhibited a lower Si/Al molar ratio than HM (Si/Al = 12.8). The tetrahedral Al have been inevitably removed during the alkali desiliconization process, and the nonframework Al species, which were formed via the hydrolysis of the displaced framework Al, might have been deposited on the mordenite framework or blocked the channel, thus rendering certain acidic sites inaccessible; the increase in the number of acid sites via the mild acid treatment, which agrees with the results in the literature,[19,42] might be a confirmation of this assumption. The total acid content of Ni−Ce/Mix acid/Na−HM was almost unchanged (Table 2) probably because the electron density was increased via the effect of the Ce cations on the polarization and induction of the silicon hydroxyl and aluminum hydroxyl groups in the framework of the molecular sieves, which offsets the negative effect of some acid sites that were covered by the Ni metal species.[31,32,52]

The Fourier-transform infrared spectroscopy of pyridine (Py-FTIR) spectra of the parent and modified HM samples in the range of 1575−1400 cm^{-1} and at 150 °C are shown in Figure 8. The B/L ratios of the parent and modified HM samples were calculated via their corresponding molar extinction coefficients[53] and integrated area of the PyH^+ and PyL bands; the results are listed in Table 2. Compared with the HM sample, the B/L ratio of the Na−HM sample decreased, while that of the Mix acid/Na−HM sample increased. The results indicated that the alkali desiliconization treatment damaged the Si−O−Si and Si−O−Al bonds, causing the transformation of the framework Al into nonframework Al and generating additional Lewis acid sites.[54,55] The B/L ratio increased after the latter step of mixed pickling, indicating that the mild mixed pickling favored the leaching of the nonframework Al, which corresponded to the NMR results. The value of the B/L ratio of the Ni−Ce/Mix acid/Na−HM sample decreased slightly probably because of the strong electron-acquiring ability of Ce^{4+}, which increased the amount of the Lewis acid.[31]

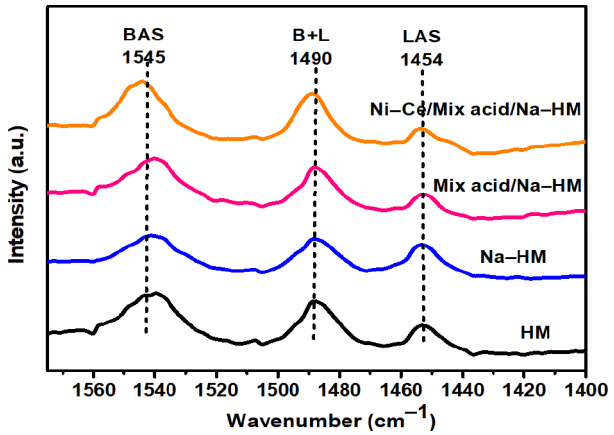

Figure 8. Py-FTIR spectra of the parent and modified HM samples.

Morphological Properties. Transmission electron microscopy (TEM) with high-resolution TEM (HR-TEM) is the most direct and valuable technique for observing and analyzing the pore structures of materials. Regarding the parent HM (Figure 9a,b), only intergranular mesopores were significantly observed, while the intragranular ones were observed in the Na−HM (Figure 9c,d) and Mix acid/Na−HM (Figure 9e,f) samples. In particular, many cavities with a size of 5−20 nm were observed in the images of the Mix acid/Na−HM samples. Additionally, the HR-TEM images (Figure 9b,d,f) exhibited the lattice fringes of the micropores. The energy-dispersive spectroscopy (EDS) mapping diagram of the micro-mesoporous HM sample that was loaded with Ni and Ce (Figure 10) revealed that elemental Ni and Ce were uniformly scattered on the surface of the sample. Therefore, the sample produced a mesoporous structure and retained the original microporous structure of the parent HM after alkali and alkali−acid treatment, and these results correspond to those obtained through XRD and N_2 sorption.

Evaluation of the Catalytic Performance. The C_9 aromatic mixture (Table 5) was catalytically isomerized in the presence of HM, Na−HM, and Mix acid/Na−HM catalysts. Following the literature,[56] the equilibrium compositions of the ET isomers are presented in Table 3. The composition of the ET isomers in the C_9 aromatic mixture deviated from the thermodynamic equilibrium value; for example, the O-ET content was much higher than the

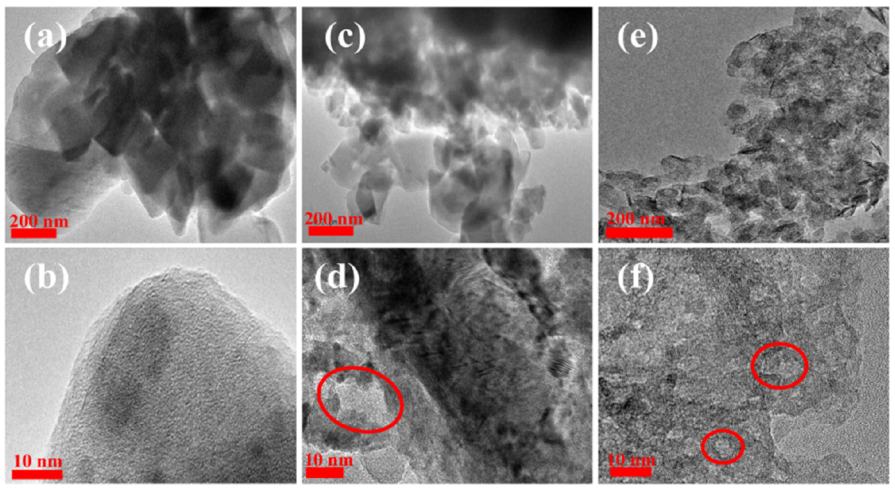

Figure 9. TEM images of (a,b) HM, (c,d) Na−HM, and (e,f) Mix acid/Na−HM.

https://doi.org/10.1021/acsomega.1c02809
ACS Omega 2021, 6, 22688−22699

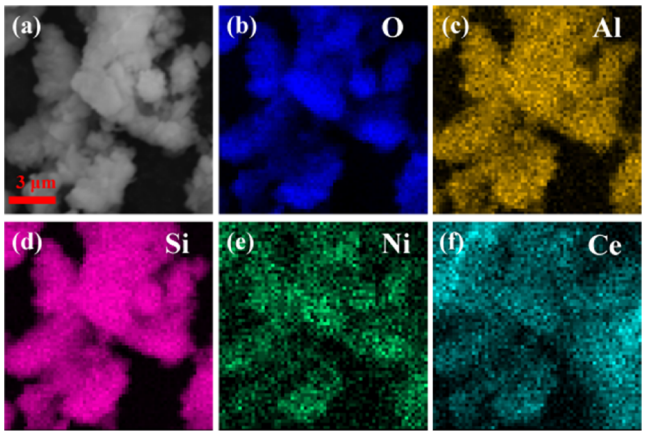

Figure 10. EDS-mapping results of the Ni−Ce/Mix acid/Na−HM sample: (a) scanning electron microscope image, (b) oxygen element distribution diagram, (c) aluminum element distribution diagram, (d) silicon element distribution diagram, (e) nickel element distribution diagram, and (f) cerium element distribution diagram.

Table 3. Composition of the Thermodynamic Equilibrium of the Ethyltoluene Isomers

	equilibrium distribution[56]	
components	315 °C	400 °C
O-ET	15.7	17.7
M-ET	50.3	50.2
P-ET	34.0	32.1

thermodynamic equilibrium composition, thus favoring the conversion of O-ET into M-ET and P-ET. Figure 11 shows the functional relationship between the yields of the products and byproducts of O-ET isomerization employing HM, Na−HM, and Mix acid/Na−HM with the reaction temperature. The product distribution for each catalyst at the optimal reaction temperature is presented in Table 4.

First, regarding the parent HM, the M-ET and P-ET yields increased with the increasing reaction temperature (a maximum value of 49.03% at 235 °C, Figure 11a), after which it decreased owing to the nonselective disproportionation, alkylation, and pyrolysis reactions, which were confirmed by the continuous increase of the byproducts (Figure 11b). Additionally, the increase of M-ET and P-ET yields of the Na−HM sample, following the alkali treatment, was not very significant in the discussed temperature range; they reached the maximum value at 215 °C. Compared with the parent HM, the M-ET and P-ET yields increased from 49.03% to 50.42%. The catalytic behavior of the desiliconized Na−HM sample was similar to that reported by Monteiro et al.,[26] indicating that the alkali desliconization treatment of the parent HM did not significantly improve the catalytic efficiency of the MOR zeolites. This result is attributable to the positive effects of increasing the mesopore volume and external surface area, which might be offset by the negative effects of the nonframework Al species covering a part of the active sites or blocking the channel. Finally, compared with the parent and Na−HM, the M-PT and P-ET yields following successive alkali and mixed-acid treatments (Mix acid/Na−HM sample) increased significantly from 33.99% to 53.60% at lowered temperatures (165 °C) (Figure 11a). This phenomenon indicated that mild mixed-acid leaching could significantly improve the catalytic performance. Moreover, the apparent

Table 4. Results of the Isomerization of O-ET Employing Different Catalysts with a ±0.5% Error at the Optimal Reaction Temperature of Each Catalyst

		product distribution[a] (%)										
sample	reaction temperature (°C)	C_1−C_6	toluene	xylene	M-, P-ET	O-ET	tri-MB	tetra-MB	PTB	others	M-ET, P-ET yield (%)	carbon mass balance[b] (%)
HM	235	0.3	0.8	1.4	22.3	3.6	64.8	2.9	0.6	3.4	49.0	99.5
Na−HM	215	0.2	0.7	1.2	22.5	3.9	65.0	2.7	0.6	3.2	50.4	99.5
Mix acid/Na−HM	165	0.2	0.8	0.9	22.8	4.0	66.4	1.7	0.6	2.7	53.6	99.6
Ni−Ce/Mix acid/Na−HM	165	0.5	1.2	2.0	22.6	4.2	65.5	2.5	0.5	0.9	51.1	98.8
[5]M-2 composite mordenite[c]	353	/[d]	/	/	/	/	/	/	/	/	45.0	/
[7]HZSM-5[c]	350	/	/	/	/	/	/	/	/	/	10.0	/
[7]Hβ[c]	350	/	/	/	/	/	/	/	/	/	24.0	/

[a]Main products of the conversion of O-ET: C_1−C_6 (alkanes and benzene); xylene (*o*-, *m*-, and *p*-xylene); M-, P-ET (*m*-, *p*-ethyltoluene); O-ET (*o*-ethyltoluene); tri-MB (trimethylbenzene isomers); tetra-MB (tetramethylbenzene isomers); PTB (pentamethylbenzene isomers), and others (macromolecular aromatics). [b](Total carbon after the reaction/total carbon before the reaction) × 100%. [c]Mean results in the literature. [d]/, not reported in the literature.

https://doi.org/10.1021/acsomega.1c02809
ACS Omega 2021, 6, 22688−22699

Table 5. Composition of the C_9 Aromatics[a]

component	M-ET	P-ET	O-ET	TMB	others
content/%	11.4	5.5	11.1	66.4	5.6

[a]M-ET, P-ET, O-ET, TMB, and others represent *m*-ethyltoluene, *p*-ethyltoluene, *o*-ethyltpoluene, trimethylbenzene, and the other components, which were obtained via GC analysis, respectively.

rate constant (k) of the O-ET isomerization reaction was 0.792 min^{-1} at 165 °C, and this was 1.8 and 1.7 times higher than those of the parent HM and Na−HM (Figure 12), respectively. Based on the Arrhenius equation (eq 3), the pre-exponential factor (A) or activation energy of the reaction could be increased or reduced to increase the apparent reaction-rate constant, respectively. Therefore, in this work, the SSAs, mesoporous volumes, and active acid sites of the Mix acid/Na−HM sample were the highest compared with those of HM and Na−HM; it corresponds to an increase in the number of active sites per unit mass of the catalyst at the same reaction-space velocity. Hence, the increase in the k value was due to an increase in the pre-exponential factor in the Arrhenius equation (Table 1). Additionally, the yields of the byproducts of the disproportionation, transalkylation, and pyrolysis reactions were <10% because of the high isomerization selectivity at temperatures of ≤165 °C (Figure 11b). The alkali−mixed acid treatment was highly efficient probably because of the removal of the nonframework Al through the mixed acid, which significantly increased the external surface area and mesoporous volume and shortened the main pores of the 12-member ring[19] to improve the mass transfer and increase the accessibility of the acid sites in nonrestrictive micropores. Concurrently, the selectivity of the isomerized products of Mix acid/Na−HM was higher than those of HM and Na−HM (Figure 11c) under the same conversion of O-ET. Csicsery and Hickson[57] confirmed that the Brønsted and Lewis acid centers are the active centers for catalyzing intramolecular and intermolecular transalkylation, respectively. Thus, the increase in the isomerization selectivity was due to an increase in the B/L ratio that was obtained through the mixed-acid treatment. Therefore, it could be concluded that high-efficiency catalysts must feature a combination of high acid-site accessibility, external surface area, mesopore volume, and B/L value in this reaction. Additionally, Table 2 reveals the selectivities of the parent and modified mordenite samples toward the target products at largely the same active state. The ratios of P-ET/M-ET for all the catalysts were less than the thermodynamic equilibrium in the following order: HM > Na−HM > Mix acid/Na−HM. Following the isomerization mechanism, O-ET was isomerized via the transfer of 1,2-alkyl in the following decreasing order of mesoporous volume for the catalysts: Mix acid/Na−HM > Na−HM > HM. However, the residence time of M-ET (the direct isomerization product of O-ET) in the pore was inverse; this benefitted the conversion of M-ET into P-ET. Notably, in the existing reports[5,7] on the catalytic isomerization of mixed ethyltoluene, the Mix acid/Na−HM achieved the lowest reaction temperature, as well as highest M-ET and P-ET yields (Table 4), exhibiting a good value for industrial applications.

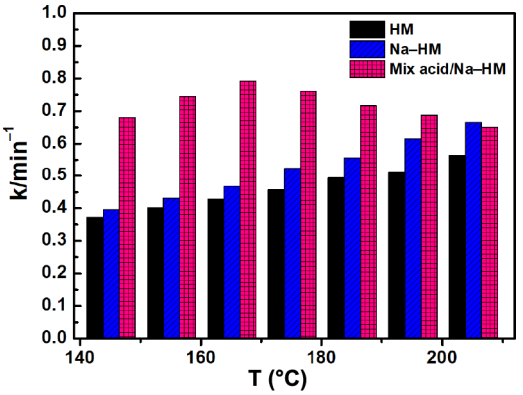

Figure 12. Apparent rate constant, k (min^{-1}), for the isomerization of O-ET employing the parent and modified HM. The data are averages of three experiments. The maximum standard deviation of each data was <2.0%.

Finally, the activity and stability of the metal-supported, alkali−mixed acid-treated catalyst (Ni/Mix acid/Na−HM and Ni−Ce/Mix acid/Na−HM) were further investigated at a low temperature (Figure 13). The curves show that the yield of the initial isomerization product of Ni−Ce/Mix acid/Na−HM was lower than that of Mix acid/Na−HM because of the presence of the Ni and Ce species, which reduced the SSA and mesopore volume, as well as the B/L value, as determined by the N_2 sorption, NH_3-TPD, and Py-FTIR analyses. After 36 h of reaction, Ni−Ce/Mix acid/Na−HM did not exhibit significant deactivation, while Mix acid/Na−HM obviously did. The XPS analysis revealed that the Ni species mainly existed as Ni^0, which exhibited a certain hydrogenation ability.

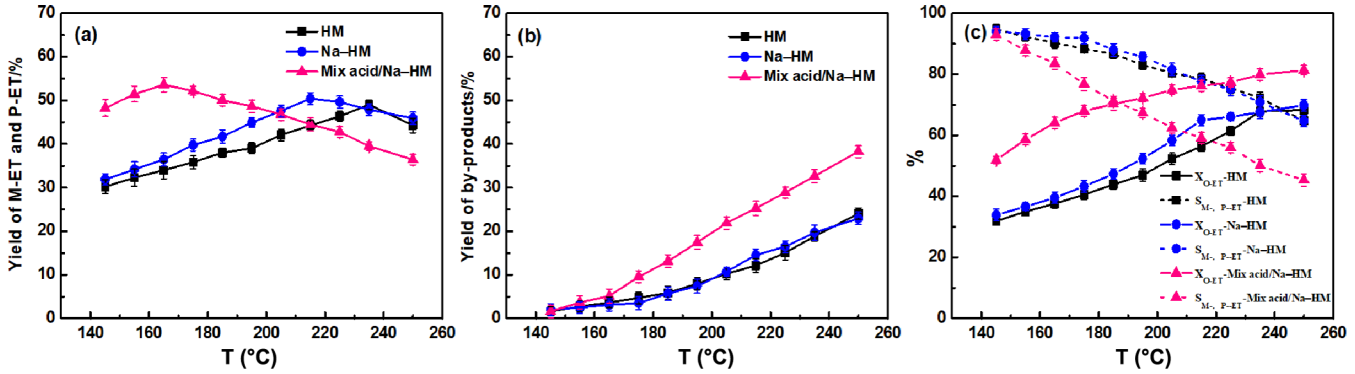

Figure 11. Catalytic activities of the parent and modified HM samples in the isomerization of O-ET as a function of temperature: (a) M-ET and P-ET yields, (b) byproduct yields, and (c) conversion of O-ET and selectivities toward M-ET and P-ET. The maximum standard deviation of each data was <2.0%.

https://doi.org/10.1021/acsomega.1c02809
ACS Omega 2021, 6, 22688−22699

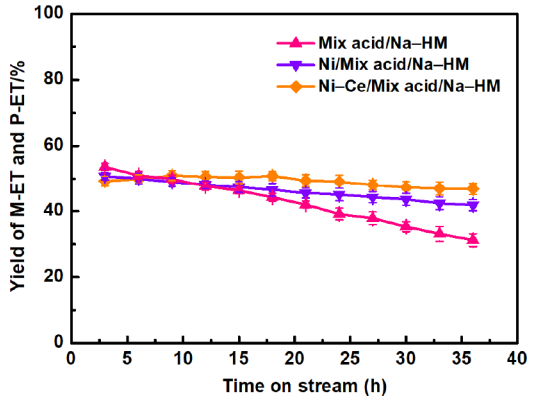

Figure 13. Dependence of the M-ET and P-ET yields on the time on stream for the isomerization of O-ET with Ni/Mix acid/Na−HM and Ni−Ce/Mix acid/Na−HM at 165 °C. The maximum standard deviation of each data was <2.0%.

Many studies[25,30] have revealed that the byproducts of macromolecular aromatics can be cracked to produce monocyclic aromatics or even alkanes via the metal and acid sites, thereby reducing the blockage of the pores. These experiments also demonstrated that Ni−Ce/Mix acid/Na−HM exhibited a better catalyst life than the single-loaded one (Ni/Mix acid/Na−HM) probably because the addition of Ce benefitted the dispersion of Ni on the catalyst, reduced the agglomeration of Ni, and further improved the inhibition of coking.

Possible Mechanism for the Isomerization of Ethyltoluene. Based on the characterization of the catalyst, as well as the results of characterizing the catalytic performance, a possible mechanism was proposed for the isomerization of O-ET, as shown in Figure 14. The main reaction consisted of the isomerization of O-ET employing the parent and modified HM to generate M-ET and P-ET, the target products Prod-1 (Figure 14) and Prod-2 (Figure 14). This transformation could be ascribed to the presence of many Brønsted acidic sites on the zeolites,[58] which protonated O-ET and formed a δ-complex (a). Owing to the instability of (a) and the higher mobility of the ethyl group than the methyl group,[56] the intramolecular transfer of the ethyl group mainly proceeded afterward from the ortho to meta positions of the methyl group, forming a new δ-complex (b), which was further transferred to the para position of the methyl group to form another δ-complex (c). According to ref 57, the direct isomerization of O-ET into P-ET via the intramolecular mechanism is impossible. Finally, M-ET (Prod-1, Figure 14) and P-MT (Prod-2, Figure 14) were obtained through deprotonation. Additionally, the *o*-toluene ethylidene carbonium ion species (d) were formed from O-ET via hydride abstraction because of the Lewis acid sites. Thereafter, yet another δ-complex (e) was selectively formed electronically and spatially, and a further δ-complex (f) was formed by the migration of the proton to other benzene rings. This migrated proton was subsequently transformed into toluene and diethyltoluene (Prod-3, Figure 14) through disproportionation or into different xylene and tetratoluene isomers for the different positions of nucleophilic substitution (Table 4). These molecules were the major byproducts that might undergo further reactions to produce higher polynuclear aromatics,[58] thereby blocking the pores in the catalyst and causing its deactivation (Table 4).

Based on all of the results of our analyses, Mix acid/Na−HM was adjudged to exhibit a high mesoporous volume, SSA, and acid content, which improved the mass transfer performance of the molecule, thereby significantly improving the catalytic performance and enabling the reaction to proceed at a lower temperature. Moreover, Mix acid/Na−HM exhibited the highest B/L value, which reduced the occurrence of side reactions; it demonstrated the highest isomerization selectivity among all of the studied catalysts. However, the increased volume of the pores as well as the external surface area also enabled the generation of macromolecular byproducts, which could not adequately improve the stability of the catalyst. Therefore, by loading the metals, Ni and Ce, as well as the macromolecular aromatics under the synergy of the metal and acid sites, the ring-opening reaction proceeded and yielded monocyclic aromatics and chain alkanes; thus, the stability of the catalyst was enhanced (Table 4).

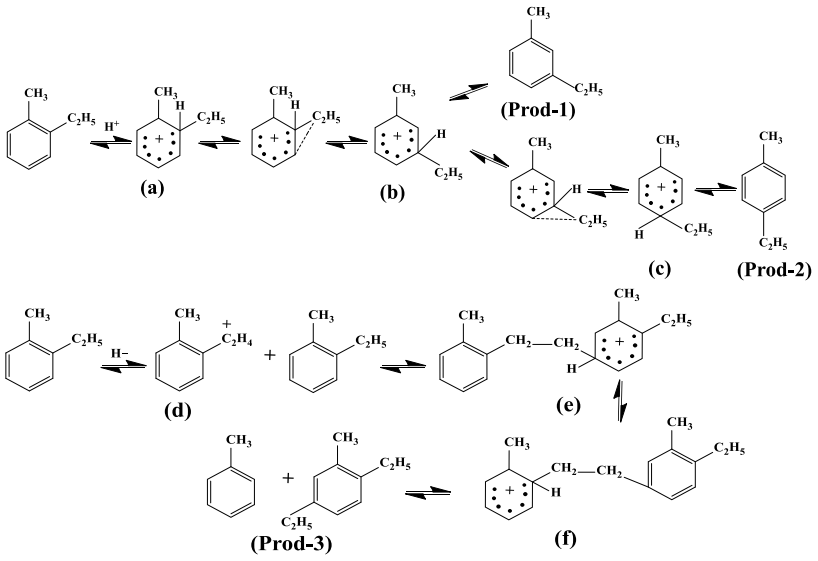

Figure 14. Mechanism of the isomerization of O-ET.

https://doi.org/10.1021/acsomega.1c02809
ACS Omega 2021, 6, 22688−22699

CONCLUSIONS

Micro-mesoporous mordenite, which was obtained from HM, was prepared via post-treatment with alkali and alkali−acid. After evaluating the isomerization performance of O-ET in the C_9 aromatics, it was observed that Mix acid/Na−HM, which was obtained after the alkali−mixed acid treatment, exhibited a significantly enhanced catalytic activity, achieving 53.60% yields of M-ET and P-ET at a lower temperature (165 °C). The apparent reaction rate constant of Mix acid/Na−HM was 1.8 and 1.7 times higher than those of parent HM and Na−HM at 165 °C, respectively, demonstrating a higher catalytic activity. The significant improvement in the catalytic performance of Mix acid/Na−HM was attributed to the removal of some nonframework Al, thus increasing the mesoporous ratio, increasing the SSA, and shortening the main channel, as well as increasing the accessibility of the acid sites. Moreover, the auxiliary active component (Ce) ensured that the active metal component (Ni) was distributed uniformly on the micro-mesoporous mordenite, thus endowing Ni−Ce/Mix acid/Na−HM with improved catalytic stability. This work offers a new strategy for further exploring the potential industrial applications of micro-mesoporous mordenite zeolites with Ni−Ce loading in the isomerization of O-ET employing C_9 aromatics as a raw material process.

EXPERIMENTAL SECTION

Materials. Nickel nitrate hexahydrate ($Ni(NO_3)_2{\cdot}6H_2O$) and cerium nitrate hexahydrate ($CeN_3O_9{\cdot}6H_2O$) were purchased from Zhenxin Reagent Co., Ltd. Sodium hydroxide (NaOH), nitric acid (HNO_3, 65%), and oxalic acid ($C_2H_2O_4$) were purchased from Sinopharm Chemical Reagent Co., Ltd. Commercial mordenite was purchased from Nankai Chemist Catalyst Co., Ltd. All of the chemicals (analytical grade) were utilized without further purification.

Preparation of the Catalyst. The commercial mordenite (labeled HM) was modified into micro-mesoporous mordenite via alkali and alkali−acid treatments. The HM sample was refluxed with a solution of 0.2 M NaOH with a liquid-to-solid ratio of 25 mL g^{-1} for 1.0 h at 75 °C. Afterward, it was filtered, washed until it attained pH 7, and ion-exchanged with 1.0 M NH_4Cl (this new sample was labeled Na−HM). The Na−HM sample was treated with a 0.1 mol L^{-1} solution of mixed HNO_3−$C_2H_2O_4$ ($C_2H_2O_4/HNO_3$ = 1:1) in a liquid-to-solid ratio of 25 mL g^{-1} for 1.0 h at 70 °C. Thereafter, it was filtered and washed to pH 7 (this sample was named Mix acid/Na−HM). Similarly, the Na−HM samples that were treated with $C_2H_2O_4/HNO_3$ = 0.5:1 and 1.5:1 were denoted as (0.5)Mix acid/Na−HM and (1.5)Mix acid/Na−HM, respectively. The sample, which was obtained via a single 0.1 M HNO_3 treatment, was denoted as NA/Na−HM. Before the experiments, all of the samples were calcined in air for 5 h at 550 °C. Ce and Ni were loaded onto the micro-mesoporous mordenite via incipient wetness impregnation employing the $CeN_3O_9{\cdot}6H_2O$ and $Ni(NO_3)_2{\cdot}6H_2O$ solutions to yield 1.25 wt % Ce and 0.5 wt % Ni (labeled Ni−Ce/Mix acid/Na−HM). Ni−Ce/Mix acid/Na−HM was activated in the following flow mixture: 100 mL min^{-1} H_2 and 100 mL min^{-1} N_2 for 4 h at 450 °C.

Characterizations. The crystallinity of the zeolite samples was analyzed via XRD (Bruker AXSD8 Advance diffractometer). The XRD patterns were obtained by Ni-filtered Cu Kα radiation (λ = 0.1541 nm) in the 2θ range of 5°−50° at a scanning rate of 5° min^{-1}. The porosity of the zeolite samples was measured via N_2 sorption employing a Micromeritics ASAP 2460 instrument. The molar ratios of the bulk Si/Al in the zeolite samples were determined via ICP-OES employing a Thermo IRIS Intrepid II XSP spectrometer. ^{27}Al and ^{29}Si MAS-NMR analyses were performed with a 4 mm probe at 35 °C employing a Bruker Avance AMS-400 spectrometer at a spinning rate of 12 kHz. The peak-fitting signals of the ^{27}Al and ^{29}Si MAS-NMR chemical shifts were referenced to $(NH_4)Al(SO_4)_2{\cdot}12H_2O$ and octakis(trimethylsiloxy)silsesquioxane, respectively, and treated by a Gaussian function. NH_3-TPD was performed on a Micromeritics AutoChem II 2920 instrument that was equipped with a TCD to study the amount and strength of the acid sites of the zeolite samples. The surface acidity was characterized by Py-FTIR on a Vertex 70 (Bruker, Germany) spectrometer that was equipped with an MCT-A detector. After the desorption of pyridine via evacuation for 1 h at 150 °C, the IR spectra of the zeolite samples were obtained by deducting the blank IR spectrum. The internal pore structures, microscopic sizes, and distributions of the Ni and Ce metals in the molecular sieve samples were analyzed via TEM and EDS-mapping employing a JEOL JEM-2100 microscope and a Hitachi S-4800 scanning electron microscope, respectively. The valence states of Ni and Ce in the catalyst were studied on an ESCA spectrometer (VG Scientific Ltd.) employing Al Kα as the X-ray source. The XPS spectrum decomposition was performed according to the binding energies of Ni and Ce. The Thermo Avantage software with Gaussian function was employed after the subtraction of the Shirley background.

Catalytic Tests. The isomerization reactions of O-ET were performed in a fixed-bed reactor. The catalyst (2.5 g) with a particle size of 60−80 mesh diameter was placed into the reactor (inner diameter = 10 mm) for the catalytic experiments. The C_9 aromatics (Table 5) were fed into the preheating section at a flow rate of 0.05 mL min^{-1} employing a metering pump. The products were obtained and detected per hour via gas chromatography (GC, Thermo Fisher Trace 1300) employing a capillary column (SE-30). The experimental conditions were as follows: temperature = 140−250 °C, pressure = 1.5 MPa, H_2/HC = 5.0 mol min^{-1}, and WHSV = 1.0 h^{-1}. GC−MS (Varian 3800/2200) equipped with a Varian cp-sil-19 column was employed to identify the products. Based on the preferential isomerization mechanism of O-ET,[30] this study focused on the isomerization process of ET. The conversion of O-ET ($X_{O\text{-}ET}$), selectivities toward M-ET and P-ET ($S_{M\text{-}ET,P\text{-}ET}$), and the yields of M-ET and P-ET ($\eta_{M\text{-}ET,P\text{-}ET}$) were calculated by eqs 1−3, respectively, where $W_{1,i}$ is the mass of O-ET in the feed, $W_{1,u}$ is the mass of O-ET in the product, and W_2 is the mass of the generated M-ET and P-ET.

Furthermore, the apparent reaction rate constant, k (min^{-1}), is another indicator for evaluating the activity of a catalyst. The isomerization of monocyclic aromatic hydrocarbons followed the first-order kinetics.[59] Therefore, k (min^{-1}) could be calculated by the rate equation of the first-order reaction (eq 4), and the pre-exponential factor (A) can be obtained via the Arrhenius equation (eq 5), which is as follows:

$$X_{O\text{-}ET} = \frac{W_{1,i} - W_{1,u}}{W_{1,i}} \times 100\% \quad (1)$$

https://doi.org/10.1021/acsomega.1c02809
ACS Omega 2021, 6, 22688−22699

$$S_{\text{M-ET,P-ET}} = \frac{W_2}{W_{1,i} - W_{i,u}} \times 100\% \quad (2)$$

$$\eta_{\text{M-ET,P-ET}} = \frac{W_2}{W_{1,i}} \times 100\% \quad (3)$$

$$k = \frac{1}{t} \cdot \ln \frac{1}{1 - \eta_{\text{M-ET,P-ET}}} \quad (4)$$

$$\ln k = -\frac{E_a}{R} \times \frac{1}{T} + \ln A \quad (5)$$

AUTHOR INFORMATION

Corresponding Authors

Zhenggui Gu − *School of Chemistry and Materials Science, Nanjing Normal University, Nanjing 210023, China; Jiangsu Provincial Key Laboratory of Materials Cycling and Pollution Control, Nanjing Normal University, Nanjing 210023, China*; Email: 07160@njnu.edu.cn

Fang Wang − *School of Chemistry and Materials Science, Nanjing Normal University, Nanjing 210023, China; Jiangsu Provincial Key Laboratory of Materials Cycling and Pollution Control and Center of Analysis and Testing, Nanjing Normal University, Nanjing 210023, China*; orcid.org/0000-0001-6086-5215; Email: wangfang@njnu.edu.cn

Authors

Xiaoyan Cao − *School of Chemistry and Materials Science, Nanjing Normal University, Nanjing 210023, China; Jiangsu Provincial Key Laboratory of Materials Cycling and Pollution Control, Nanjing Normal University, Nanjing 210023, China*; orcid.org/0000-0003-4625-2281

Ruiyun Wang − *School of Chemistry and Materials Science, Nanjing Normal University, Nanjing 210023, China; Jiangsu Provincial Key Laboratory of Materials Cycling and Pollution Control, Nanjing Normal University, Nanjing 210023, China*

Kaijun Wang − *School of Chemistry and Materials Science, Nanjing Normal University, Nanjing 210023, China; Jiangsu Provincial Key Laboratory of Materials Cycling and Pollution Control, Nanjing Normal University, Nanjing 210023, China*

Complete contact information is available at: https://pubs.acs.org/10.1021/acsomega.1c02809

Notes

The authors declare no competing financial interest.

ACKNOWLEDGMENTS

The authors acknowledge financial support from the National Natural Science Foundation of China (no. 21973045), China Petroleum & Chemical Corporation (no. J418013-3), and the Jiangsu scientific and technological transformative project (no. SBA2018030374). The related measure and analysis instrument for this work were supported by the Centre for Analysis, Nanjing Normal University.

REFERENCES

(1) Firth, M. J. Derivation of a chronic reference dose and reference concentration for trimethylbenzenes and C_9 aromatic hydrocarbon solvents. *Regul. Toxicol. Pharmacol.* **2008**, *52*, 248−256.

(2) Serra, J. M.; Guillon, E.; Corma, A. A rational design of alkyl-aromatics dealkylation−transalkylation catalysts using C_8 and C_9 alkyl-aromatics as reactants. *J. Catal.* **2004**, *227*, 459−469.

(3) Tukur, N. M.; Al-Khattaf, S. Catalytic Transformation of 1,3,5-Trimethylbenzene over a USY Zeolite Catalyst. *Energy Fuels* **2007**, *21*, 2499−2508.

(4) Ko, A. N.; Kuo, C. T. Isomerization and Disproportionation of 1,2,4-Trimethylbenzene over HY Zeolite. *J. Chem. Soc.* **1994**, *41*, 145−150.

(5) Wang, I.; Tsai, T. C.; Huang, S. T. Disproportionation of toluene and of trimethylbenzene and their transalkylation over zeolite beta. *Ind. Eng. Chem. Res.* **1990**, *29*, 2005−2012.

(6) Nishi, H.; Moffat, J. B. Catalysis by microporous heteropoly oxometalates: The conversion of 1-methyl-2-ethylbenzene. *J. Mol. Catal.* **1989**, *51*, 193−207.

(7) Cheng, X.; Wang, X.; Long, H. Transalkylation of benzene with 1,2,4-trimethylbenzene over nanosized ZSM-5. *Microporous Mesoporous Mater.* **2009**, *119*, 171−175.

(8) Liu, L.; Jin, F.; Xiong, G.; Long, H.; Wang, X. Facile synthesis and catalytic applications of micro-mesoporous molecular sieve ZK-1. *J. Porous Mater.* **2013**, *20*, 637−645.

(9) Meier, W. M. The crystal structure of mordenite (ptilolite). *Z. Kristallogr. - Cryst. Mater.* **1961**, *115*, 439−450.

(10) Csicsery, S. M. Selective disproportionation of alkylbenzenes over mordenite molecular sieve catalyst. *J. Catal.* **1970**, *19*, 394−397.

(11) Tromp, M.; Van Bokhoven, J. A.; Garriga Oostenbrink, M. T.; Bitter, J. H.; De Jong, K. P.; Koningsberger, D. C. Influence of the Generation of Mesopores on the Hydroisomerization Activity and Selectivity of n-Hexane over Pt/Mordenite. *J. Catal.* **2000**, *190*, 209−214.

(12) Jung, J. S.; Park, J. W.; Seo, G. Catalytic cracking of n-octane over alkali-treated MFI zeolites. *Appl. Catal., A* **2005**, *288*, 149−157.

(13) Tao, Y.; Kanoh, H.; Abrams, L.; Kaneko, K. Mesopore-Modified Zeolites: Preparation, Characterization, and Applications. *Chem. Rev.* **2006**, *106*, 896−910.

(14) Li, Y.; Liu, S.; Zhang, Z.; Xie, S.; Zhu, X.; Xu, L. Aromatization and isomerization of 1-hexene over alkali-treated HZSM-5 zeolites: Improved reaction stability. *Appl. Catal., A* **2008**, *338*, 100−113.

(15) Cheung, P.; Bhan, A.; Sunley, G. J.; Iglesia, E. Selective Carbonylation of Dimethyl Ether to Methyl Acetate Catalyzed by Acidic Zeolites. *Angew. Chem., Int. Ed.* **2006**, *45*, 1617−1620.

(16) Tzoulaki, D.; Jentys, A.; Perez-Ramirez, J.; Egeblad, K.; Lercher, J. A. On the location, strength and accessibility of Bronsted acid sites in hierarchical ZSM-5 particles. *Catal. Today* **2012**, *198*, 3−11.

(17) Wang, Y.; Lancelot, C.; Lamonier, C.; Richard, F.; Leng, K.; Sun, Y.; Rives, A. Hierarchization of Mordenite as NiW Sulfide Catalysts Support: Towards Efficient Hydrodesulfurization. *ChemCatChem* **2015**, *7*, 3936−3944.

(18) Li, X.; Prins, R.; Van Bokhoven, J. A. Synthesis and characterization of mesoporous mordenite. *J. Catal.* **2009**, *262*, 257−265.

(19) Pastvova, J.; Kaucky, D.; Moravkova, J.; Rathousky, J.; Sklenak, S.; Vorokhta, M.; Brabec, L.; Pilar, R.; Jakubec, I.; Tabor, E.; Klein, P.; Sazama, P. Effect of Enhanced Accessibility of Acid Sites in Micromesoporous Mordenite Zeolites on Hydroisomerization of n-Hexane. *ACS Catal.* **2017**, *7*, 5781−5795.

(20) Huang, Z.; Zhang, J.; Han, Q.; Zhang, X.; Lu, P.; Xu, L.; Yuan, Y.; Xu, L. Promoting effects of desilication and dealumination on the catalytic performance of Al-rich HMOR for catalysing naphthalene tert-butylation with tertiary butanol. *Appl. Catal., A* **2019**, *572*, 80−89.

(21) Bai, G.; Li, T.; Yang, Y.; Zhang, H.; Lan, X.; Li, F.; Han, J.; Ma, Z.; Chen, Q.; Chen, G. Microwave-assisted Friedel−Crafts acylation of indole with acetic anhydride over tungstophosphoric acid modified Hβ zeolite. *Catal. Commun.* **2012**, *29*, 114−117.

(22) Giudici, R.; Kouwenhoven, H. W.; Prins, R. Comparison of nitric and oxalic acid in the dealumination of mordenite. *Appl. Catal., A* **2000**, *203*, 101−110.

(23) Boily, J. F.; Qafoku, O.; Felmy, A. R. A potentiometric, spectrophotometric and pitzer ion-interaction study of reaction

equilibria in the aqueous H^+-Al^{3+}, H^+-oxalate and H^+-Al^{3+}-oxalate systems up to 5 mol·dm−3 NaCl. *J. Solution Chem.* **2007**, *36*, 1727−1743.
(24) Sun, H.; Huang, X.; Wang, F.; Gu, Z. Impact of acidic properties of HBEA zeolite on isomerization of 1-methylnaphthalene. *Res. Chem. Intermed.* **2017**, *43*, 4697−4710.
(25) Tsai, T.-C.; Chen, W.-H.; Liu, S.-B.; Tsai, C.-H.; Wang, I. Metal zeolites for transalkylation of toluene and heavy aromatics. *Catal. Today* **2002**, *73*, 39−47.
(26) Monteiro, R.; Ania, C. O.; Rocha, J.; Carvalho, A. P.; Martins, A. Catalytic behavior of alkali-treated Pt/HMOR in n-hexane hydroisomerization. *Appl. Catal., A* **2014**, *476*, 148−157.
(27) Nagy, E.; Fetting, F. Zur Kinetik der Isomerisierung von n-Hexan an H-Mordenit mit 0,5% Pt-Gehalt. *Chem. Ing. Tech.* **1981**, *53*, 729−731.
(28) Law, P. L.; Kenney, C. N. Pentane isomerization kinetics over nickel-loaded Y-type zeolite. *J. Catal.* **1980**, *64*, 241−250.
(29) Wang, S.; Guo, W.; Zhu, L.; Wang, H.; Qiu, K.; Cen, K. Methyl Acetate Synthesis from Dimethyl Ether Carbonylation over Mordenite Modified by Cation Exchange. *J. Phys. Chem. C.* **2015**, *119*, 524−533.
(30) Wang, Y.; Wang, M.; Zhang, X. Study on the isomerization performance of trimethylbenzene on Ni-Mo/HM. *Chem. Ind. Eng.* **2016**, *33*, 35−39.
(31) Ning, Q.; Zhang, H. K.; He, Y. R.; Chen, Z. Q.; Liu, S. Y.; Ren, J. Suppression of platinum sintering on Pt-M/ZSM-22 (M = Ce, La, and Re) catalyst for n-dodecane isomerization. *New J. Chem.* **2019**, *43*, 13967−13978.
(32) Park, S.-H.; Rhee, H.-K. Shape selective conversion of 1,2,4-trimethylbenzene over zeolite NU-87. *Catal. Today* **2000**, *63*, 267−273.
(33) Odedairo, T.; Balasamy, R.; Al-khattaf, S. Aromatic transformations over aluminosilicate micro/mesoporous composite materials. *Catal. Sci. Technol.* **2012**, *2*, 1275−1286.
(34) Lv, J.; Hua, Z.; Zhou, J.; Liu, Z.; Guo, H.; Shi, J. Surface-Passivated Hierarchically Structured ZSM5 Zeolites: High-Performance Shape-Selective Catalysts for para-Xylene Production. *ChemCatChem* **2018**, *10*, 2278−2284.
(35) Zhou, H.; Zhu, W. L.; Shi, L.; Liu, H. C.; Liu, S. P.; Xu, S. T.; Ni, Y. M.; Liu, Y.; Li, L.; Liu, Z. M. Promotion effect of Fe in mordenite zeolite on carbonylation of dimethyl ether to methyl acetate. *Catal. Sci. Technol.* **2015**, *5*, 1961−1968.
(36) Triwahyono, S.; Jalil, A. A.; Musthofa, M. Generation of protonic acid sites from pentane on the surfaces of Pt/SO_4^{2-}-ZrO_2 and Zn/H-ZSM5 evidenced by IR study of adsorbed pyridine. *Appl. Catal., A* **2010**, *372*, 90−93.
(37) Van Laak, A. N. C.; Sagala, S. L.; Zečević, J.; Friedrich, H.; De Jongh, P. E.; De Jong, K. P. Mesoporous mordenites obtained by sequential acid and alkaline treatments − Catalysts for cumene production with enhanced accessibility. *J. Catal.* **2010**, *276*, 170−180.
(38) Verboekend, D.; Mitchell, S.; Milina, M.; Groen, J. C.; Pérez-Ramírez, J. Full Compositional Flexibility in the Preparation of Mesoporous MFI Zeolites by Desilication. *J. Phys. Chem. C.* **2011**, *115*, 14193−14203.
(39) Sazama, P.; Sobalik, Z.; Dedecek, J.; Jakubec, I.; Parvulescu, V.; Bastl, Z.; Rathousky, J.; Jirglova, H. Enhancement of Activity and Selectivity in Acid-Catalyzed Reactions by Dealuminated Hierarchical Zeolites. *Angew. Chem., Int. Ed.* **2013**, *52*, 2038−2041.
(40) Lietz, G.; Schnabel, K. H.; Peuker, C.; Gross, T.; Storek, W.; Volter, J. Modifications of H-ZSM-5 Catalysts by NaOH Treatment. *J. Catal.* **1994**, *148*, 562−568.
(41) Leng, K.; Wang, Y.; Hou, C.; Lancelot, C.; Lamonier, C.; Rives, A.; Sun, Y. Enhancement of catalytic performance in the benzylation of benzene with benzyl alcohol over hierarchical mordenite. *J. Catal.* **2013**, *306*, 100−108.
(42) Bonilla, A.; Baudouin, D.; Pérez-Ramírez, J. Desilication of ferrierite zeolite for porosity generation and improved effectiveness in polyethylene pyrolysis. *J. Catal.* **2009**, *265*, 170−180.
(43) Liu, X. Y.; Wang, K.; Zhou, Y.; Tang, X. Y.; Zhu, X. H.; Zhang, R. S.; Zhang, X. L.; Jiang, X.; Liu, B. D. In-situ fabrication of noble metal modified (Ce, Zr)O2−δ monolithic catalysts for CO oxidation. *Appl. Surf. Sci.* **2019**, *483*, 721−729.
(44) Yang, T.-S.; Chang, T.-H.; Yeh, C.-T. Acidities of sulfate species formed on a superacid of sulfated alumina. *J. Mol. Catal. A: Chem.* **1997**, *115*, 339−346.
(45) Pan, Y. X.; Hu, G. H.; Lu, J. T.; Xiao, L.; Zhuang, L. Ni(OH)2-Ni/C for hydrogen oxidation reaction in alkaline media. *J. Energy Chem.* **2019**, *29*, 111−115.
(46) Trovarelli, A. Catalytic Properties of Ceria and CeO2-Containing Materials. *Chem. Rev.* **1996**, *38*, 439−520.
(47) Navarro, R. M.; Álvarez-Galván, M. C.; Rosa, F.; Fierro, J. L. G. Hydrogen production by oxidative reforming of hexadecane over Ni and Pt catalysts supported on Ce/La-doped Al_2O_3. *Appl. Catal., A* **2006**, *297*, 60−72.
(48) Bai, G. Y.; Ma, Z.; Shi, L. J.; Li, T. Y.; Han, J.; Chen, G. F.; Li, N.; Liu, P. D. An effective lactic acid-modified Hβ zeolite for synthesis of bis(indolyl)methanes. *Res. Chem. Intermed.* **2012**, *38*, 2501−2510.
(49) Esquivel, D.; Cruz-Cabeza, A. J.; Jimenez-Sanchidrian, C.; Romero-Salguero, F. J. Enhanced Concentration of Medium Strength Brönsted Acid Sites in Aluminium-Modified β Zeolite. *Catal. Lett.* **2012**, *142*, 112−117.
(50) Corma, A. Inorganic Solid Acids and Their Use in Acid-Catalyzed Hydrocarbon Reactions. *Chem. Rev.* **1995**, *95*, 559−614.
(51) Srivastava, R.; Iwasa, N.; Fujita, S.; Arai, M. Dealumination of Zeolite Beta Catalyst Under Controlled Conditions for Enhancing its Activity in Acylation and Esterification. *Catal. Lett.* **2009**, *130*, 655−663.
(52) Noda, T.; Suzuki, K.; Katada, N.; Niwa, M. J. Combined study of IRMS-TPD measurement and DFT calculation on Brønsted acidity and catalytic cracking activity of cation-exchanged Y zeolites. *J. Catal.* **2008**, *259*, 203−210.
(53) Emeis, C. A. Determination of Integrated Molar Extinction Coefficients for Infrared Absorption Bands of Pyridine Adsorbed on Solid Acid Catalysts. *Catal. Today* **1993**, *141*, 347−354.
(54) Ordomsky, V. V.; Ivanova, I. I.; Knyazeva, E. E.; Yuschenko, V. V.; Zaikovskii, V. I. Cumene disproportionation over micro/mesoporous catalysts obtained by recrystallization of mordenite. *Catal. Today* **2012**, *295*, 207−216.
(55) Svelle, S.; Sommer, L.; Barbera, K.; Vennestrøm, P. N. R.; Olsbye, U.; Lillerud, K. P.; Bordiga, S.; Pan, Y.-H.; Beato, P. How defects and crystal morphology control the effects of desilication. *Catal. Today* **2011**, *168*, 38−47.
(56) Csicsery, S. Equilibrium distributions of the dimethylethylbenzene and methyldiethylbenzene isomers. *J. Chem. Eng. Data* **1967**, *12*, 118−122.
(57) Csicsery, S. M.; Hickson, D. A. Selectivities of acid-catalyzed reactions over silica-alumina and molecular sieve catalysts. *J. Catal.* **1970**, *19*, 386−393.
(58) Rombi, E.; Monaci, R.; Solinas, V. Kinetics of catalyst deactivation. An example: Methylnaphthalene transformation. *Catal. Today* **1999**, *52*, 321−330.
(59) Tukur, N. M.; Al-Khattaf, S. Comparison studies of xylene isomerization and disproportionation reactions between SSZ-33, TNU-9, mordenite and ZSM-5 zeolite catalysts. *Chem. Eng. J.* **2011**, *166*, 348−357.

https://doi.org/10.1021/acsomega.1c02809
ACS Omega 2021, 6, 22688−22699